MICRO-435 Quantum and Nanocomputing

Edoardo Charbon
Mariagrazia Graziano

September 30, 2025

Quantum Computing Syllabus (Week 1-7)

- Fundamentals of quantum computing
- **Qubit realization & control**
- Cryo-CMOS components
- Scalable quantum computers
- Quantum communication, sensing, and metrology

Qubit Realization & Control (3)

- Background
- Quick superconductivity recap
- Superconducting qubits
- Design, control and readout of superconducting qubits
- Characterization of superconducting qubits
- Cryogenic control of superconducting qubits
- Spin qubits
- Readout and control of spin qubits
  - DC readout
  - RF readout
- Characterization of spin qubits
- Characterization setups
- Deriving system specifications

Acknowledgements: Simone Frasca, Andrea Ruffino, Jeroen van Dijk

Spin Qubits

Small Digression: p-n Junction

- An n-doped Si region placed in contact with a p-doped Si region forms a p-n junction
- Doping types
  - n-region is Si doped with donor atoms
  - p-region is Si doped with acceptor atoms
- Depletion layer is the volume where electrons from the n-region have escaped to fill the holes in the p-region

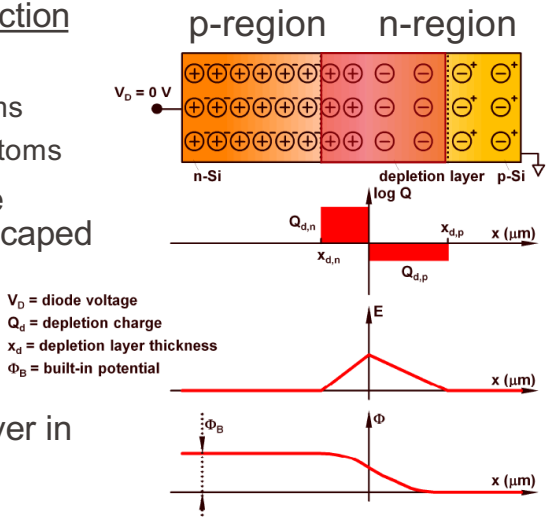

- Unlike n/p-regions, the depletion layer in ***not*** neutral

Small Digression: p-n Junction (2)

- Forward-biased junction
  - → depletion region shrinks
  - → Electric field reduces
  - → Potential becomes smaller

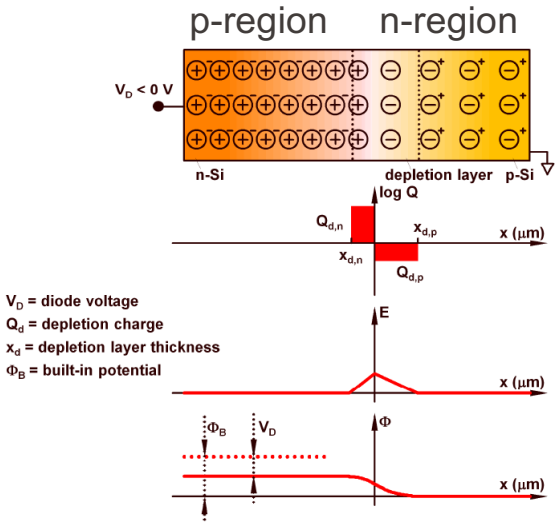

Small Digression: p-n Junction (3)

- Reverse-biased junction
  - → depletion region expands
  - → Electric field increases
  - → Potential becomes larger

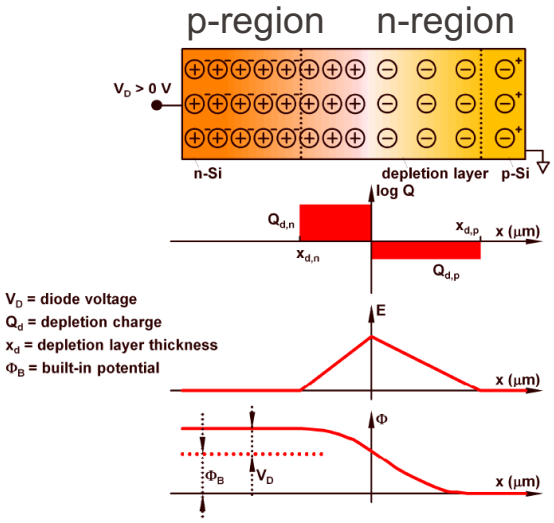

Small Digression: MOS Transistor

- The metal-oxide semiconductor (MOS) transistor is a 2-junction structure
- Source is an n^+-doped region providing charges to the channel
- Drain is an n^+-doped region draining away charges from the channel

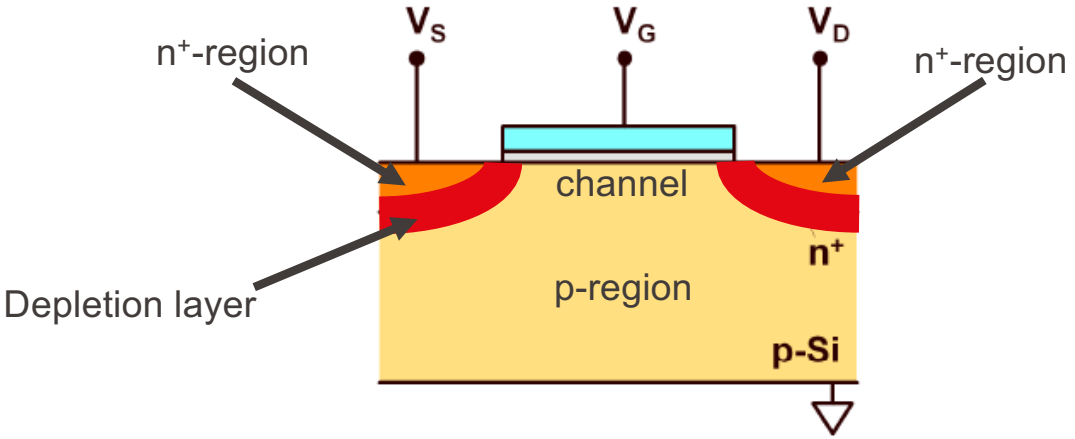

Small Digression: MOS Transistor (2)

- Gate voltage V_G at 0V
- No current through the channel

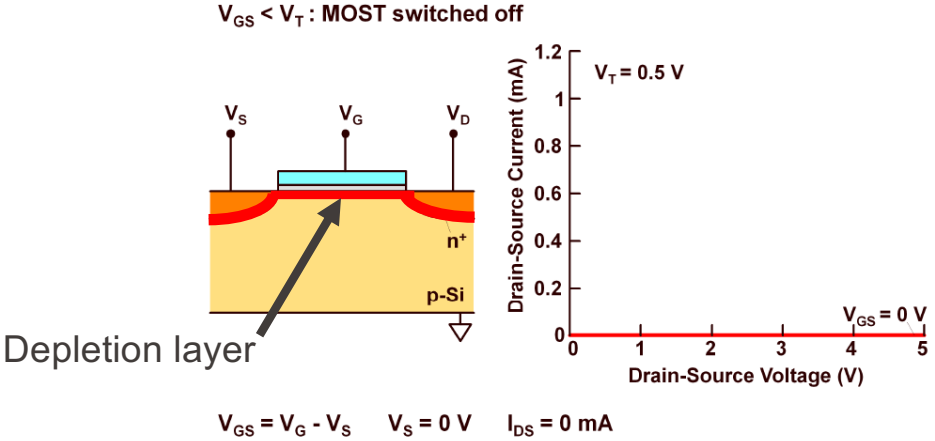

Small Digression: MOS Transistor – Linear Region

- Gate voltage V_G >0V, small voltage btw. source and drain
- A channel forms in the depletion layer under the gate
- Current through the channel is proportional to drain-source voltage

$V_{GS} > V_T$: MOST switched on : linear region

$V_{DS} < V_{GS} - V_T$

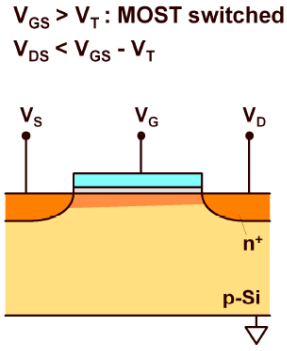

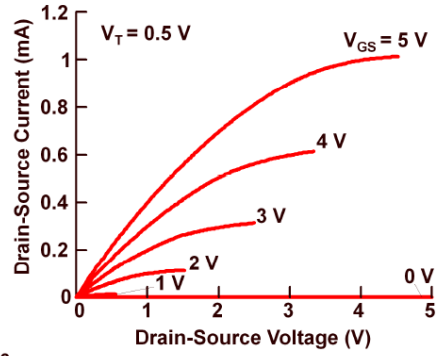

$$I_{DS} = K \cdot \left[(V_{GS} - V_T) \cdot V_{DS} - \frac{V_{DS}^2}{2} \right] \qquad K = \mu \cdot C_{ox} \cdot \frac{W}{L}$$

Small Digression: MOS Transistor – Saturation Region

- Gate voltage V_G >0V, large voltage btw. source and drain
- Channel pinch-off
- Current through the channel is saturated (like a current source)

$V_{GS} > V_T$: MOST switched on : saturation

$V_{DS} > V_{GS} - V_T$

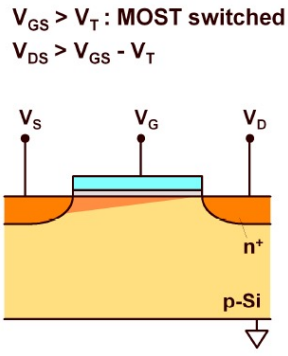

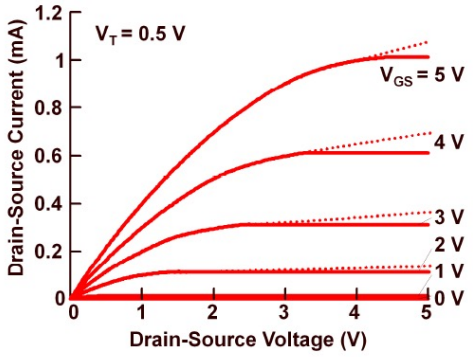

$$I_{DS} = \frac{K}{2} \cdot (V_{GS} - V_T)^2 \qquad K = \mu \cdot C_{ox} \cdot \frac{W}{L}$$

Questions

- Can control a current in the channel that has a granularity down to a single carrier?
- Can we force charge transport electron-by-electron on demand?
- If so what would be the conditions to do so?

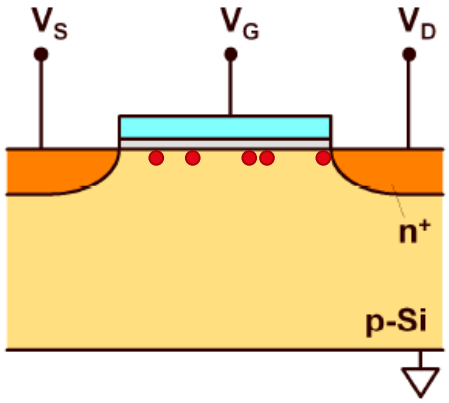

Spin Qubits: The Main Idea

- Create a quantum dot by way of a 2D electron gas (2DEG)
- Store one and only one electron in the quantum dot (QD)
- Read and control the state of the electron

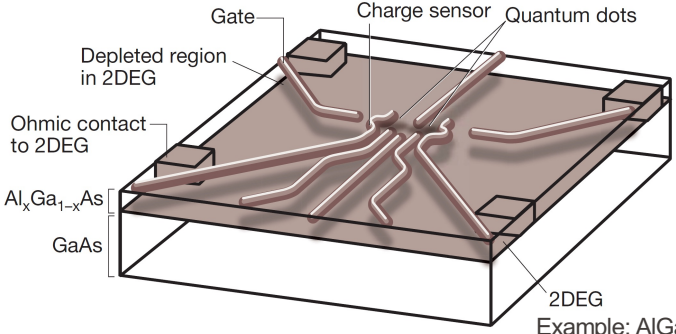

Fermi wavelength:

$$\lambda_F = \frac{2\pi}{k_F} = \sqrt{\frac{2\pi}{\rho}}$$

Example: AlGaAs-GaAs* heterostructure
Source: T. D. Ladd et al. Nature 464, 2010.

*) Advantages of these materials: single conduction band valley and a small effective mass leading to less stringent lithographic constraints

Spin Qubits: The Main Idea (2)

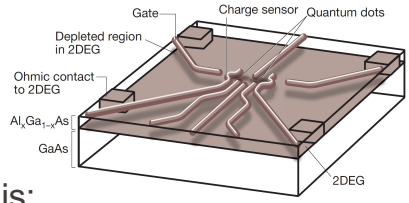

- Energy levels in the QD become quantized
- Many energy levels are possible (μ_j)
- With N electrons confined in the QD, the energy is:

$$U(N) = \frac{[-|e|(N-N_0)+\sum_i C_i V_i]^2}{2C} + \sum_J^N E_j.$$

- The electrochemical potential μ_N of the island is defined as:

$$\mu_N = U(N) - U(N-1).$$

- The energy to add an extra electron to the island is:

$E_{add} = \mu_{N+1} - \mu_N = E_c + \Delta E, \;\; E_c = e^2/C$ ** charging energy.

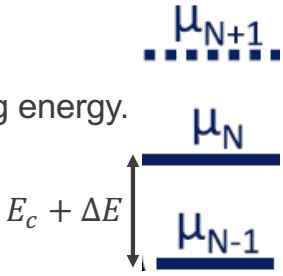

**) C is the self-capacitance of the QD.

Charge Transport Time Dynamics

- The time needed to transfer a charge to the QD is:

$$\tau = R_t C, \quad \text{where } R_t \text{ is the tunneling resistance.}$$

- Since the uncertainty principle must apply:

$$\Delta E\, \Delta t = E_c \tau > h \rightarrow\ R_t > \frac{h}{2e^2}.$$

- Also, the thermal energy levels of the electrons must be sufficiently low not to excite the electrons on or off the QD. Thus:

$k_B T < \frac{e^2}{C}$, where k_B is the Boltzmann constant and T the temperature.

Example:

For an island of 100nm (~60aF), the charging energy is ~3meV, which is 10x the thermal energy of the electron at 4K (~0.3meV).

Charge Transport Conditions

- μ_N aligns with source and drain, thus carriers can flow from the source to the drain reservoirs by tunneling and the number of electrons oscillates from N to $N-1$.
- Source-drain voltage V_{SD}, since $\mu_S - \mu_D = -|e|VSD$, and the potential on the island can be used to establish transport

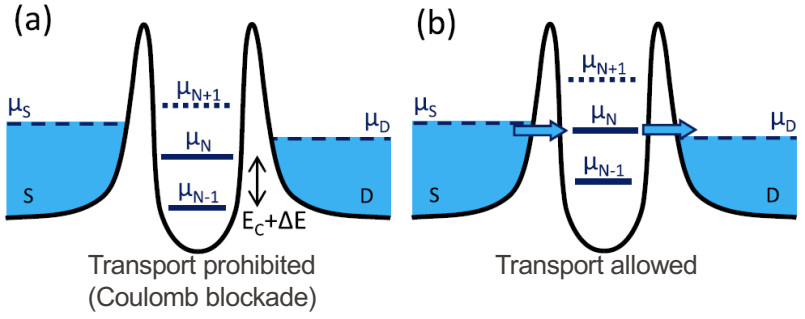

F.A. Zwanenburg et al. rev. mod. phys, 2013

Charge Transport Conditions (2)

- Schematic representation of electrochemical potential lines
- The energy of the next available state in the QD μ_N is higher than that of the highest occupied state of the reservoirs (Fermi energy).
- No electron can go to the QD.
- The line at the QD below is lower than the Fermi energy of both reservoirs, thus no electrons can leave the QD.
- No electrons can move, thus we have a Coulomb Blockade.

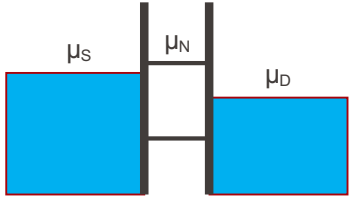

Charge Transport Conditions (3)

- Now, we add a gate at the bottom (right diagram), biased at Vg. As a result the ladder of energies can be moved down.
- Now, electrons can move, but before the first electron leaves, no second electron can enter.
- So, individual electrons can be controlled one by one.
- This results in a measurable current, which is seen on the right.

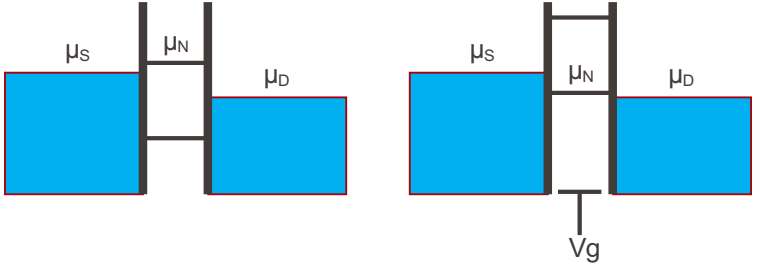

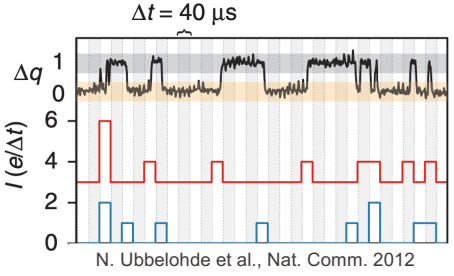

N. Ubbelohde et al., Nat. Comm. 2012

System of QDs

- Two QDs each with control gate $Vg_{1,2}$
- V_B is controlling the tunnel barrier to isolate the two electrons.

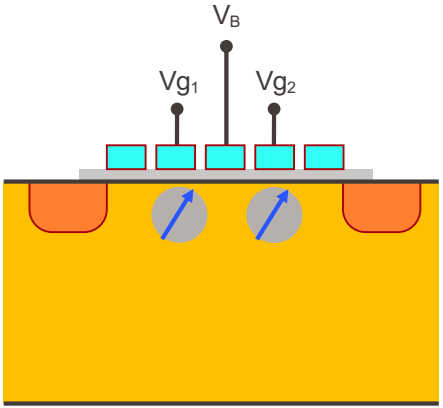

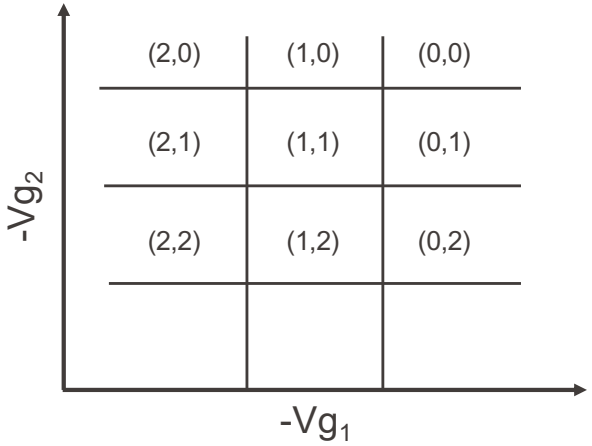

System of QDs (2)

- Considering adjacent QDs, we will see cross-talk, causing vertical and horizontal lines to be aligned at an angle.

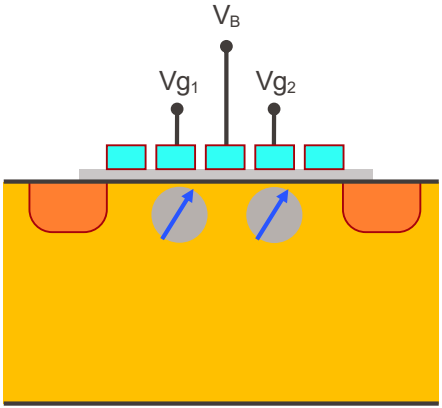

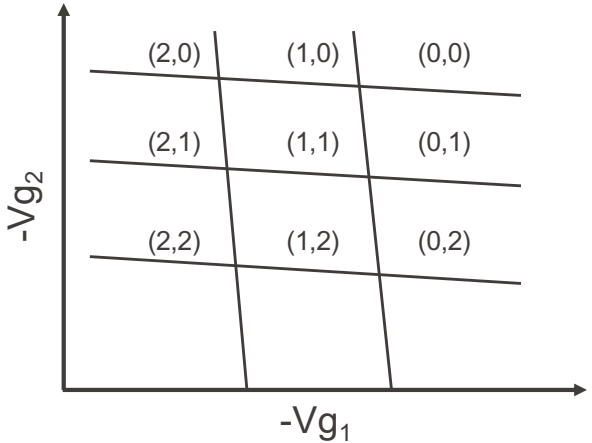

System of QDs (3)

- We will also see that a change in the number of electrons in one QD changes the alignment of the levels in the second QD.

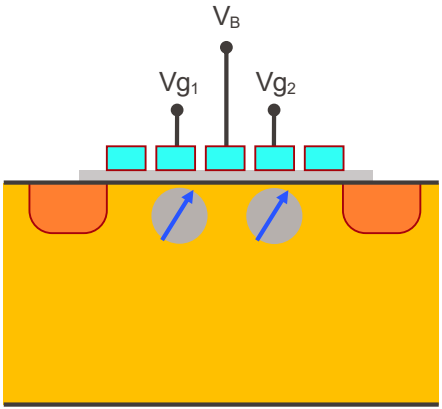

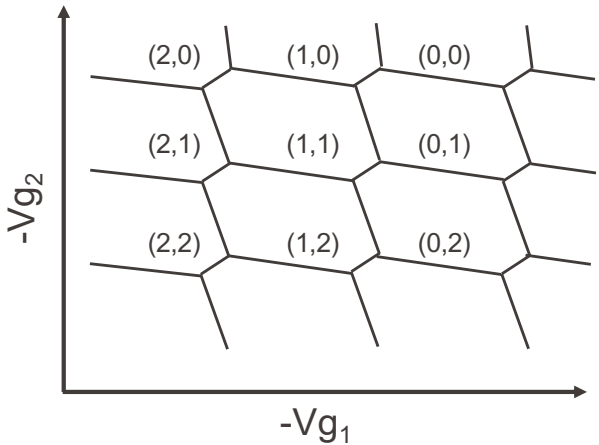

Stability Diagram

- The diagram shows the allowed transitions with its characteristic Coulomb diamonds

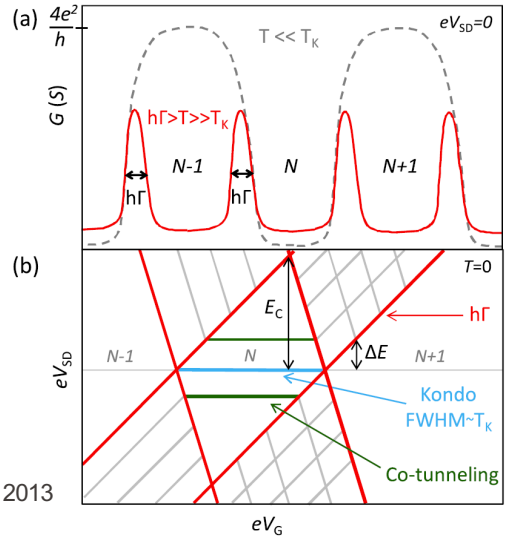

Conductance peaks

Coulomb diamonds

F.A. Zwanenburg et al. rev. mod. phys, 2013

Zeeman Splitting – Single Qubit Encoding

- The lowest energy level in a QD can be occupied by two electrons with opposite spin (Pauli's exclusion principle)
- To create a true two-level system (to represent a qubit) a DC magnetic field B_{DC} is applied to split the energy of electrons in the ground state.
- Zeeman effect: an energy $E_Z = \pm \mu_B g_L B_{DC}$ is added, where μ_B is the Bohr magneton, and g_L is the Landé g-factor.
- The resulting distinct energy states are attributed to $|0\rangle$ and $|1\rangle$.

Quantum Dot (QD)

Energy Diagram

Double QD (DQD) Encoding

- It is also possible to encode the state of the qubit in 2 QDs
- In this case, the double QD or DQD will be encoded as shown.
- The qubit is known as single—triplet qubit is robust to global magnetic field fluctuations.
- Coherent rotations can be achieved via a magnetic field gradient between the dots.

Double Quantum Dot (DQD)

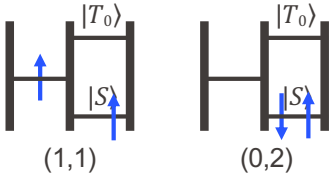

Possible DQD configurations

$$|T_0\rangle = \frac{|\uparrow\downarrow\rangle + |\downarrow\uparrow\rangle}{\sqrt{2}}$$

$$|S\rangle = \frac{|\uparrow\downarrow\rangle - |\downarrow\uparrow\rangle}{\sqrt{2}}$$

Readout and control of spin qubits

Larmor and Rabi Oscillations

- When the electron is located in static magnetic field B_{DC} in the z direction, it performs a precession around the magnetic field axis at the Larmor frequency $\omega_{Larmor} = \gamma_R B_{DC}$.
- However, a perpendicular AC magnetic field, $B(t) = BAC\cos(\omega_{mw}\, t)$ rotating at frequency $\omega = \omega_{Larmor}$ can cancel the static magnetic field, such that the spin will perform a precession around the rotating magnetic field, at the Rabi frequency $\omega_{Rabi} = \gamma_R B_{AC}$.
- In order to control the spin of the electron in the quantum dot, microwave signals with accurate amplitude and phase have to be applied.

γ_R is the gyromagnetic ratio due to the interaction of its magnetic dipole with the applied field.

Controlling Qubit State on Bloch's Sphere

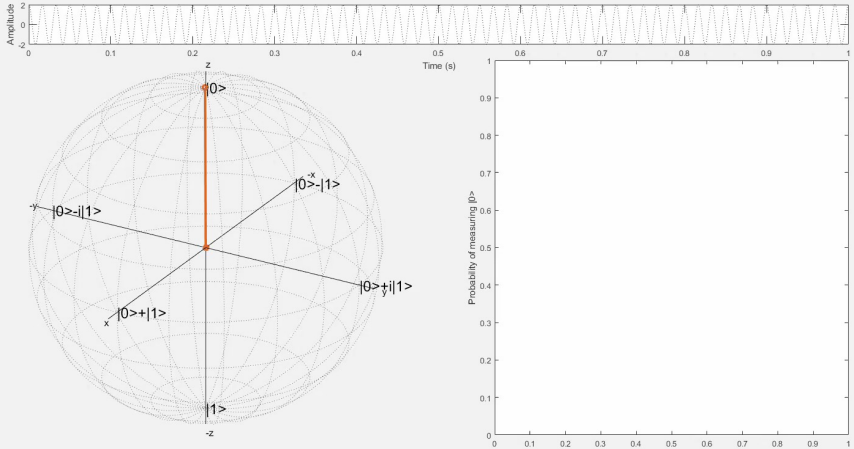

Jeroen v. Dijk

Reading Spin Qubit States

- DC techniques
  - Spin-to-charge
  - \+ Simplicity: direct readout and amplification of the transport current
  - – Limitations: $1/f$ noise and low speed due to large caps
- RF techniques
  - RF reflectometry [Reilly et al., 2007]
  - Dispersive Gate Sensing (DGS) [Colless et al., 2013].
  - \+ Robustness, accuracy
  - – Complexity

DC Readout Techniques: Single Spin

- Spin-to-charge conversion based on energy selection.
- A single spin in a QD is capacitively coupled to a sensor and tunnel coupled to a reservoir.
- The QD energy is tuned s.t. the Fermi energy of the reservoir is btw. The two Zeeman-split states (↑ and ↓).
- If the state is ↓, then Coulomb blockade prevents the electron from entering the reservoir. If it is ↑, the electron can tunnel out.

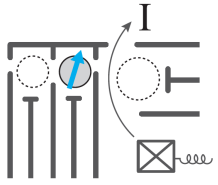

single-spin readout

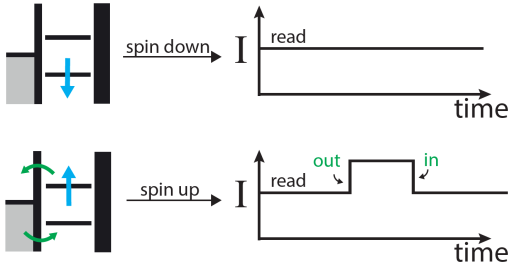

DC Readout Techniques: Double QD (DQD)

- Spin-to-charge conversion based singlet-triplet qubit.
- After spin manipulation in (1,1) state, i.e. one electron in each QD, the dot levels are tilted in favor of the (0,2) state.
- If states are ↑ and ↓, the left electron can tunnel to the same orbital occupied by the right electron, thus charge will change and detected.
- If states are the same (↑ and ↑ or ↓ and ↓), then Pauli exclusion prevents tunneling, thus no charge change.

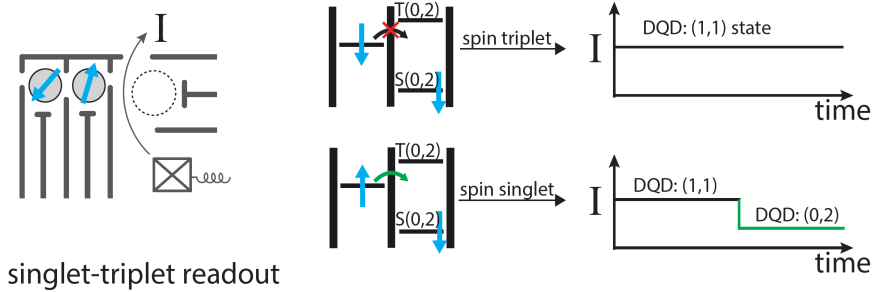

singlet-triplet readout

RF Readout Techniques: Reflectometry

- A narrow channel, called called Quantum Point Contact (QPC), or a Single-Electron Transistor (SET) is an intermediate electrometer to sense the state of the qubit and convert it into an electrical quantity, which is then read out.
- Spin-to-charge is applied to the QPC, which has quantized conductance and thus a staircase conversion gain.
- A RF signal is used to probe the QPC. The portion of the RF carrier is reflected back is proportional to the QPC charge, and thus the state of the qubit, thus the name.

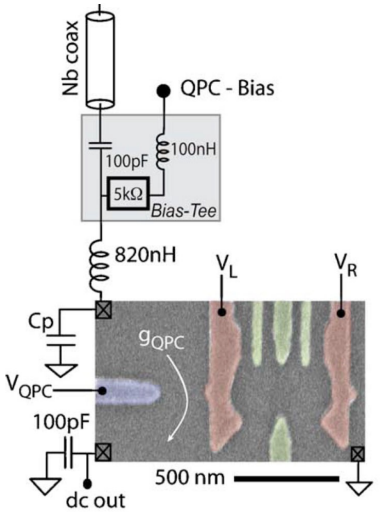

RF reflectometry

D. J. Reilly et al., *APL* 91(16), 2007.

RF Readout Techniques: Dispersive Readout

- An impedance matching network converts the high gate impedance of the QPC to 50Ω.
- Through a RF carrier signal the phase of the reflected signal is read out.
- The capacitance C_q will be modulated by the state of the qubit.
- This contributes to a phase shift $\Delta\varphi$ that is measured in the response of the resonant matching network.
- For this reason, this technique is called dispersive gate-based sensing.

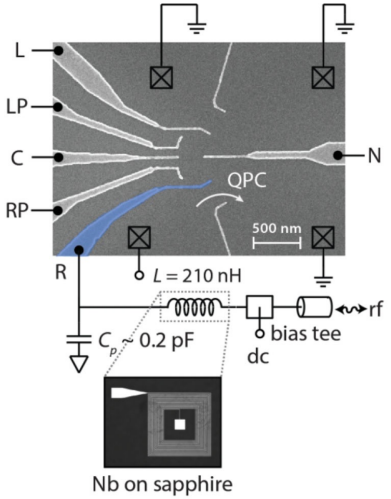

Dispersive gate sensing

J. I. Colless et al., *PRL* 110, 2013.

Characterization of spin qubits

Qubit Characterization

- Key single-qubit timescales:
  - Relaxation time T_1
  - Maximum coherence time T_2 using dynamical decoupling.
  - T_2^*
- Measurements on qubits:
  - Rabi oscillations
  - Randomized benchmarking

Important Definitions

- T_1 denotes the probability that a qubit will stay in state $|1\rangle$ after time t, given by the formula:

$$P(|1\rangle) = e^{-t/T_1}.$$

- T_2 is the so-called *decoherence time*. It describes the time required to go from $|+\rangle = \frac{1}{\sqrt{2}}(|0\rangle + |1\rangle)$ to $|-\rangle = \frac{1}{\sqrt{2}}(|0\rangle - |1\rangle)$, or how long the phase of a qubit stays intact. T_2 is an ideal performance measure.

- T_2^* is the *observed dephasing* time, such that $T_2^* < T_2$.

Measuring T_1 and T_2^*

- T_1 is measured as follows:
  1. Prepare the qubit in the excited state $|1\rangle$ by rotating in by π in the Bloch sphere.
  2. Wait some time t.
  3. Measure the state of the qubit.

- T_2 is measured as follows:
  1. Prepare the qubit in superposition state $|+\rangle = \frac{1}{\sqrt{2}}(|0\rangle + |1\rangle)$, e.g. applying a $\frac{\pi}{2}$ rotation.
  2. Wait some time t.
  3. Apply another $\frac{\pi}{2}$ rotation to bring the qubit back to the $|0\rangle$ state.
  4. Measure the state of the qubit.

Measuring T_1 and T_2^* (2)

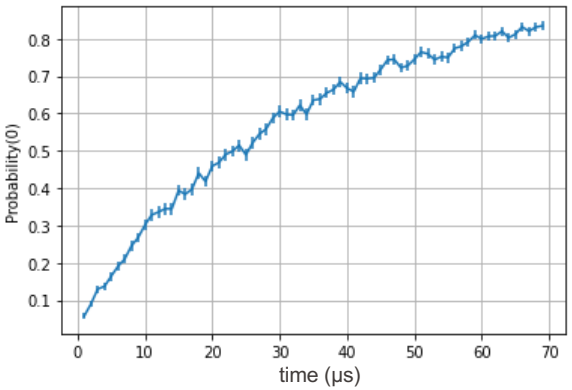

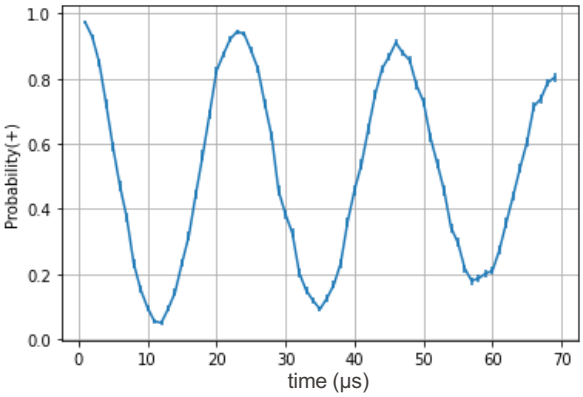

Source: Rahaf Youssef *et al.*

Rabi Cycle or Flop

- Definition: cyclic behavior of two-level quantum system in presence of oscillatory driving field.
- Measurement:
  1. Prepare qubit in superposition state, e.g. $\frac{1}{\sqrt{2}}(|0\rangle + |1\rangle)$.
  2. Measure state w.r.t. to e.g. X-direction at time t.
  3. Repeat with different values of t.
- What to we expect from the measurement?

$$|\langle +X|\psi(t)\rangle|^2 = cos^2\left(\frac{\omega t}{2}\right),$$

where $\omega = \frac{E_+ - E_-}{\hbar}$.

Electron Spin Resonance (ESR)

- In practice, Rabi oscillations are achieved in a slightly different way.
- Measurement:
  1. Prepare qubit in ground state.
  2. Rotate state using an AC B_1-field of duration τ_P to drive transitions from spin-down to spin-up. Frequency is tuned to resonate with dipole (39.1GHz).
  3. Measure state w.r.t. X-direction.
  4. Repeat with different values of τ_P.

39.1GHz

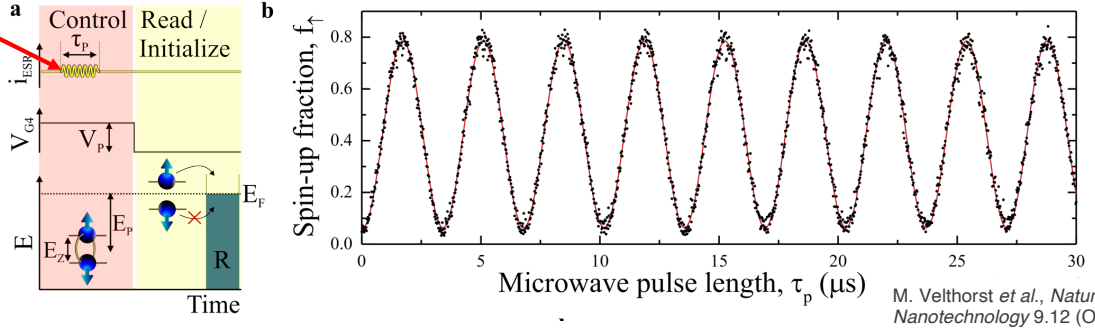

M. Velthorst *et al.*, *Nature Nanotechnology* 9.12 (Oct. 2014)

Electron Spin Resonance (2)

- Zeeman splitting is typically obtained with 1T.
- AC magnetic field B_1, which interacts with the magnetic dipole of the electron, is obtained with a current flowing through a transmission line.
- Rabi oscillations can be seen at resonance frequency.

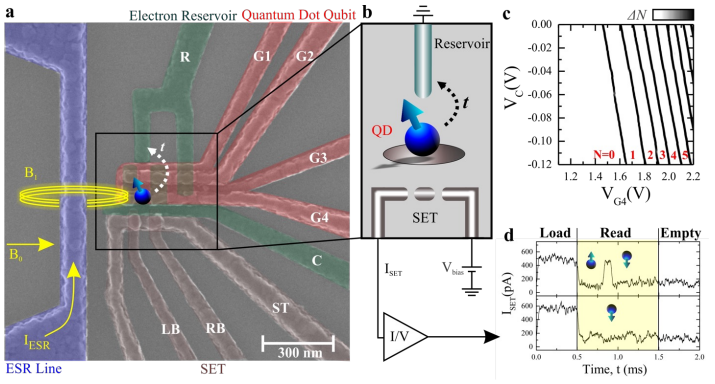

M. Velthorst *et al.*, *Nature Nanotechnology* 9.12 (Oct. 2014)

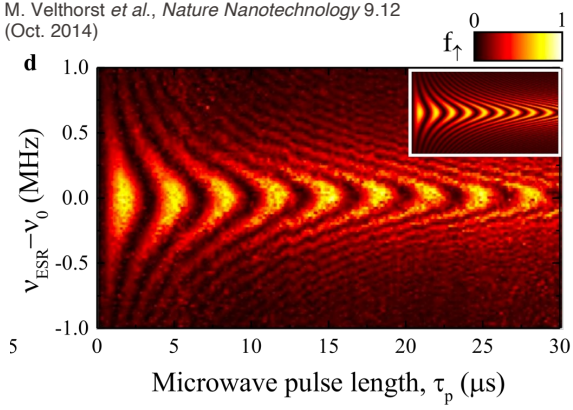

Electric Dipole Spin Resonance (EDSR)

- The same effect can be obtained by applying a varying electric field to the electron (or a hole) in a spatial magnetic field gradient.
- QDs are formed under the gate and occupancies are controlled by Vg_1 and Vg_2. ***In this case the charge is a hole.***
- Source-drain current I_{sd} is a function of magnetic field B (perpendicular to the chip) and MW frequency f.

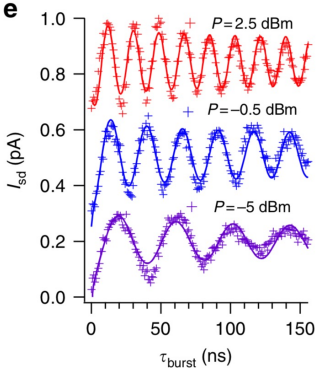

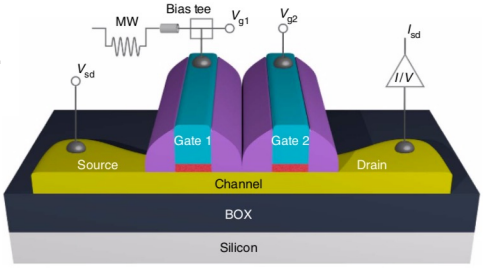

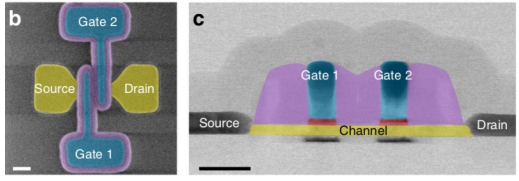

R. Maurand *et al.*, *Nature Communications* 7:13575 (Nov. 2016).

Extracting T_2^*

- When detuning, we see coherent oscillations, Ramsey fringes.
- T_2^* is extracted from the decay of the Ramsey oscillations.
- T_2^* is 1μs in natural Si and 120μs in isotopically purified Si (^{28}Si has atomic 0-spin, thus it does not interfere with the qubit state).

M. Velthorst *et al.*, *Nature Nanotechnology* 9.12 (Oct. 2014)

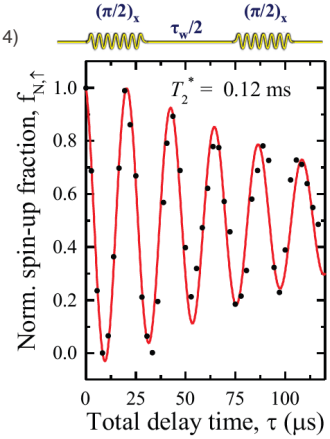

Randomized Benchmarking

- Fidelity is characterized on a large number m of Clifford gates, by means of a sequence shown here.
- From the decay, we deduce the fidelity by fitting an exponential decay.
- A π pulse of 1.6μs and a waiting time of 500ns between consecutive gates is used.

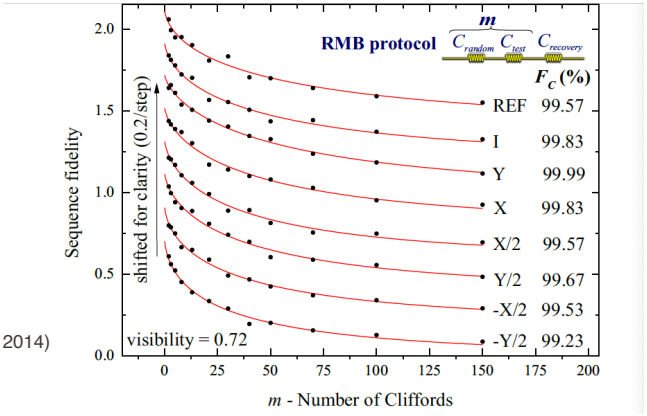

M. Velthorst *et al.*, *Nature Nanotechnology* 9.12 (Oct. 2014)

State-of-the-art Implementations of Si/SiGe Qubits

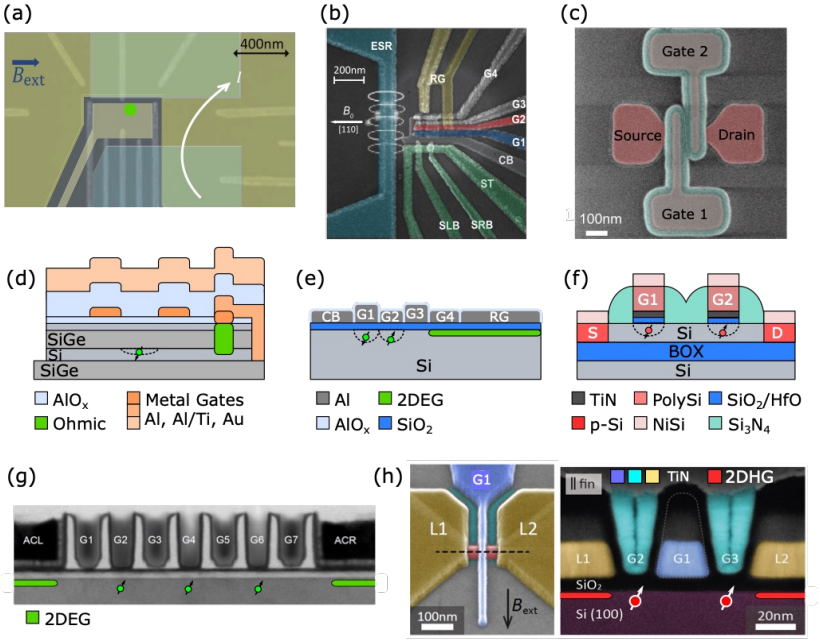

Qubit Characterization Summary

Qubit type	Characteristic timescales (s)		Quantum Computation		Quantum Sensing	
	T_1	T_2	Single-qubit gate time	Single-qubit fidelity	Quantity	Sensitivity
Gated charge	30 ns[124]	7 ns[7]	∼0.1 ns[8]	86%[124]	Charge	$\sim 10^{-4}\ \mathrm{e}/\sqrt{(\mathrm{Hz})}$ at 1 Hz[7]
Gated spin	57 s[125]	28 ms[19]	0.25 ns[20]	99.96%*[126]	Magnetic field gradients	50 pT/$\sqrt{\mathrm{Hz}}$[19,127]
Shallow dopants (electron)	> 1 h[80] (ens), 10 s[128]	10 s[83] (ens), 0.56 s[94]	∼ 100 ns[43]	99.94%*[97]	Magnetic field (AC)	18 pT/$\sqrt{\mathrm{Hz}}$[94]
Shallow dopants (nucleus)	> days[50]	3 h[88] (ens), 35.6 s[94]	∼ 20 μs[50]	99.98%*[96]	Magnetic field (AC)	2 nT/$\sqrt{\mathrm{Hz}}$[94]
Color centers	>1 h[129]	1s[129]	<20 ns[130]	99.995%*[131]	Magnetic field (DC)	50 pT/$\sqrt{\mathrm{Hz}}$[132] (ens), 500 nT/$\sqrt{\mathrm{Hz}}$[133]
					Magnetic field (AC)	32 pT/$\sqrt{\mathrm{Hz}}$[134] (ens), 4.3 nT/$\sqrt{\mathrm{Hz}}$[135]
					Temperature	100 mK/$\sqrt{\mathrm{Hz}}$[136,137]
					Electric Field	$10^{-5}\ \mathrm{V}\cdot\mu\mathrm{m}^{-1}/\sqrt{(\mathrm{Hz})}$[138]

7. Petersson, K. D., Petta, J. R., Lu, H. & Gossard, A. C. Quantum coherence in a one-electron semiconductor charge qubit. *Phys. Rev. Lett.* **105**, 246804 (2010).

8. Cao, G. *et al.* Ultrafast universal quantum control of a quantum-dot charge qubit using Landau–Zener–Stückelberg interference. *Nat Commun* **4**, 1401 (2013).

19. Veldhorst, M. *et al.* An addressable quantum dot qubit with fault-tolerant control-fidelity. *Nature* **9**, 981–985 (2014).

20. Yoneda, J. *et al.* A quantum-dot spin qubit with coherence limited by charge noise and fidelity higher than 99.9%. *Nat. Nanotech.* **13**, 102–106 (2018).

43. Pla, J. J. *et al.* A single-atom electron spin qubit in silicon. *Nature* **489**, 541 (2012).

50. Pla, J. J. *et al.* High-fidelity readout and control of a nuclear spin qubit in silicon. *Nature* **496**, 334 (2013).

80. Feher, G. & Gere, E. Electron spin resonance experiments on donors in silicon. ii. electron spin relaxation effects. *Physical Review* **114**, 1245 (1959).

83. Tyryshkin, A. M. *et al.* Electron spin coherence exceeding seconds in high-purity silicon. *Nature Materials* **11**, 143 (2012).

88. Saeedi, K. *et al.* Room-temperature quantum bit storage exceeding 39 minutes using ionized donors in silicon-28. *Science* **342**, 830–833 (2013).

94. Muhonen, J. T. *et al.* Storing quantum information for 30 seconds in a nanoelectronic device. *Nature Nanotechnology* **9**, 986 (2014).

96. Muhonen, J. *et al.* Quantifying the quantum gate fidelity of single-atom spin qubits in silicon by randomized benchmarking. *Journal of Physics: Condensed Matter* **27**, 154205 (2015).

97. Dehollain, J. P. *et al.* Optimization of a solid-state electron spin qubit using gate set tomography. *New Journal of Physics* **18**, 103018 (2016).

124. Kim, D. *et al.* Microwave-driven coherent operation of a semiconductor quantum dot charge qubit. *Nature Nanotechnology* **10**, 243–247 (2015).

125. Camenzind, L. C. *et al.* Hyperfine-phonon spin relaxation in a single-electron gaas quantum dot. *Nature Communications* **9**, 3454 (2018).

126. Yang, C. *et al.* Silicon qubit fidelities approaching incoherent noise limits via pulse engineering. *Nature Electronics* **2**, 151–158 (2019).

127. Taylor, J. M. *et al.* High-sensitivity diamond magnetometer with nanoscale resolution. *Nature Physics* **4**, 810–816 (2008).

128. Tenberg, S. B. *et al.* Electron spin relaxation of single phosphorus donors in metal-oxide-semiconductor nanoscale devices. *Physical Review B* **99**, 205306 (2019).

129. Abobeih, M. H. *et al.* One-second coherence for a single electron spin coupled to a multi-qubit nuclear-spin environment. *Nature Communications* **9**, 2552 (2018).

130. Robledo, L. *et al.* High-fidelity projective read-out of a solid-state spin quantum register. *Nature* **477**, 574–578 (2011).

131. Rong, X. *et al.* Experimental fault-tolerant universal quantum gates with solid-state spins under ambient conditions. *Nature Communications* **6**, 8748 (2015).

132. Schloss, J. M., Barry, J. F., Turner, M. J. & Walsworth, R. L. Simultaneous broadband vector magnetometry using solid-state spins. *Physical Review Applied* **10**, 034044 (2018).

133. Liu, Y.-X., Ajoy, A. & Cappellaro, P. Nanoscale vector dc magnetometry via ancilla-assisted frequency up-conversion. *Physical Review Letters* **122**, 100501 (2019).

134. Glenn, D. R. *et al.* High-resolution magnetic resonance spectroscopy using a solid-state spin sensor. *Nature* **555**, 351–354 (2018).

135. Balasubramanian, G. *et al.* Ultralong spin coherence time in isotopically engineered diamond. *Nature Materials* **8**, 383–387 (2009).

136. Anisimov, A. N. *et al.* Optical thermometry based on level anticrossing in silicon carbide. *Scientific Reports* **6**, 33301 (2016).

137. Nguyen, C. T. *et al.* All-optical nanoscale thermometry with silicon-vacancy centers in diamond. *Applied Physics Letters* **112**, 203102 (2018).

138. Michl, J. *et al.* Robust and accurate electric field sensing with solid state spin ensembles. *Nano Letters* **19**, 4904–4910 (2019).

Characterization Setups

Characterization Setups: SC Qubits

- Setups vary depending on the type of qubits and their temperature, resonance frequency, etc.
- Control signals are generated at room temperature (RT).
- Thermalization is used to reduce the noise generated at RT to what would be if generated at cryogenic temperatures.
- This requires large signals at RT to achieve pV-nV at cryo-T.

$$P = \frac{V^2}{R} \rightarrow V = \sqrt{1\mu W \times 50\Omega} = 7mV$$

$$1mW = 0dBm$$
$$1\mu W = -30dBm$$
$$1pW = -90dBm \rightarrow V = 7\mu V$$

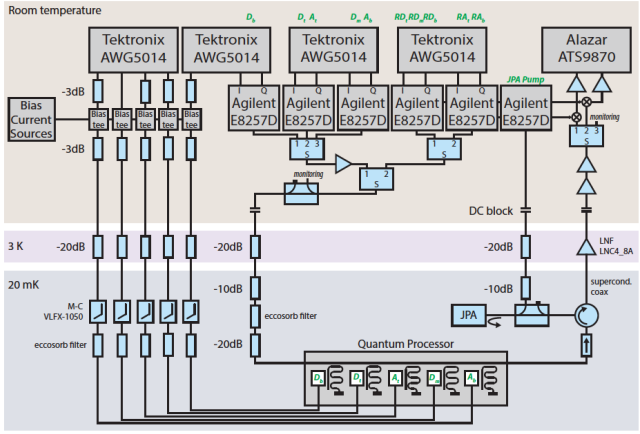

D. Ristè et al., Detecting bitflip errors in a logical qubit using stabilizer measurements', Nature Communications 6.1 (Apr. 2015).

Characterization Setups: Spin Qubits

- Frequencies here tend to be higher.
- Temperatures of qubits can reach up to 5K [Kamenzind, 2020].
- Same challenges as before in terms of thermalization

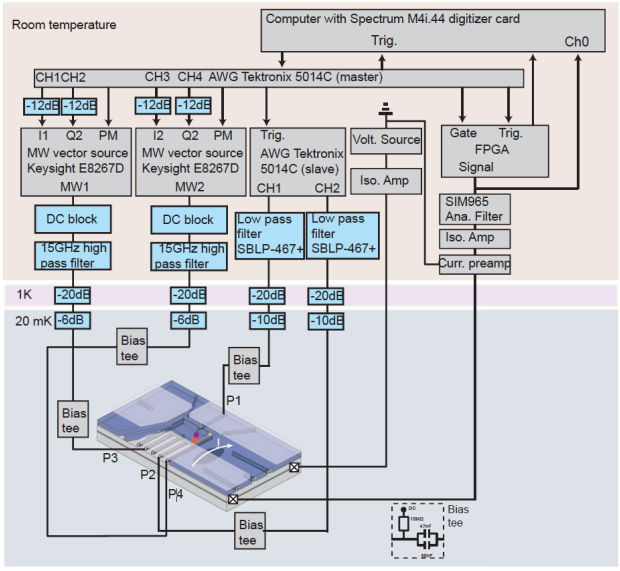

T. F. Watson et al., 'A programmable two-qubit quantum processor in silicon'. Nature 555.7698 (Feb. 2018).

Example of RF-Reflectometry

- Intermediate temperature stages.
- Directional couplers may be bulky.
- Challenges in terms of local resonators.

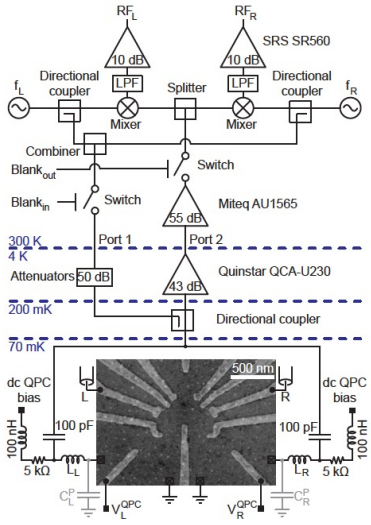

E. A. Laird et al. 'Coherent spin manipulation in an exchange only qubit', Physical Review B 82.7 (Aug. 2010).

Limitations of RT Control

- Scalability
  - Large number of qubits cannot be handled due to wiring and RT control complexity
- Reliability
  - Large and complex wiring networks makes it hard to maintain and debug
- Signal integrity
  - Large signals are needed at RT and thermalization networks are complex
- Feedback latency
  - Due to long wires and multi-stage electronics delays in the feedback control-readout systems may be long

Alternative: Cryogenic Control

- Proposed solution
  - Electronics at 4 K
  - Only connections to 4 K to 20 mK are needed

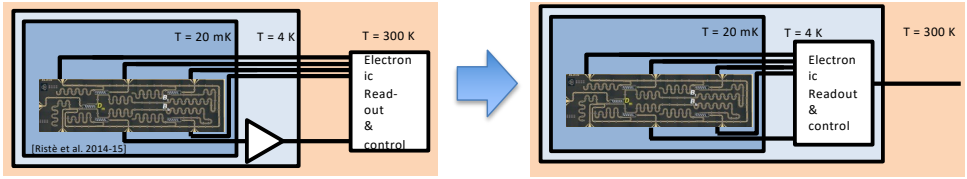

- Ultimate solution
  - Qubits at 4 K
  - Monolithic integration

Alternative: Cryogenic Control (2)

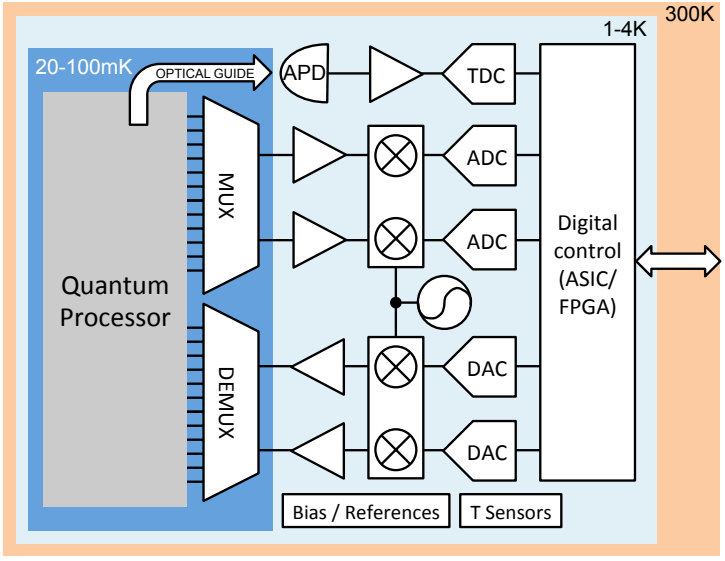

E. Charbon *et al.*, *IEDM* 2016

Approximate Specifications

- Noise budget…..... < 0.1nV/√Hz
- Power budget (for scalability)…..... << 2mW/qubit
- Physical dimensions (for scalability)…..... 30nm
- Bandwidth (for multiplexing)…..... 1-12GHz
- Kick-back avoidance

Power Issue

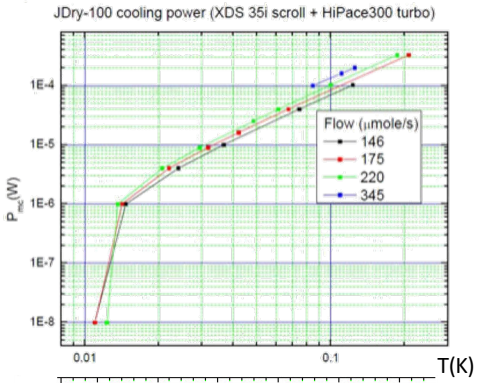

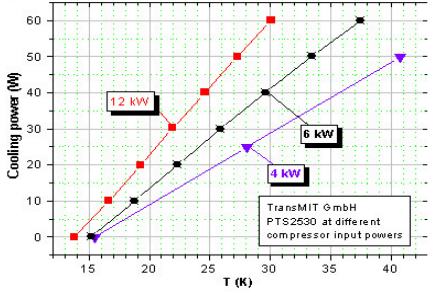

Dilution refrigerator

300 K

70 K

4 K

100 mK

20 mK

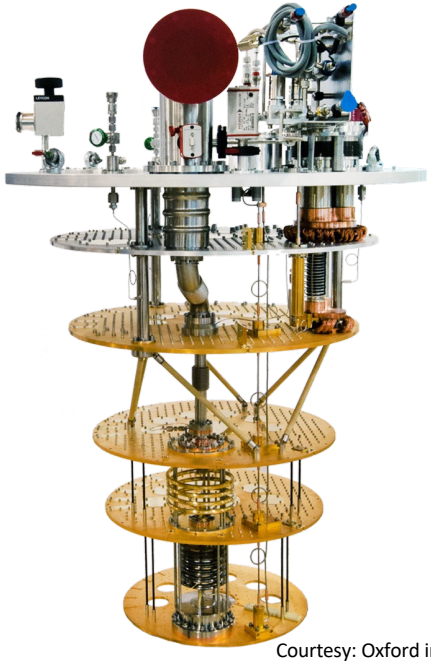

Courtesy: Oxford instruments

Deriving System Specifications

Generic Model of Spin-Qubit Quantum Processor

- External B_0 induces Zeeman splitting (energy difference E_z between ↑ and ↓.
- The electron rotates around the Z-axis in the Bloch sphere with Larmor frequency $\omega_0 = \gamma_e |B_0|$, where γ_e is the gyromagnetic ratio of the electron ($\gamma_e \approx 28$GHz/T in silicon).

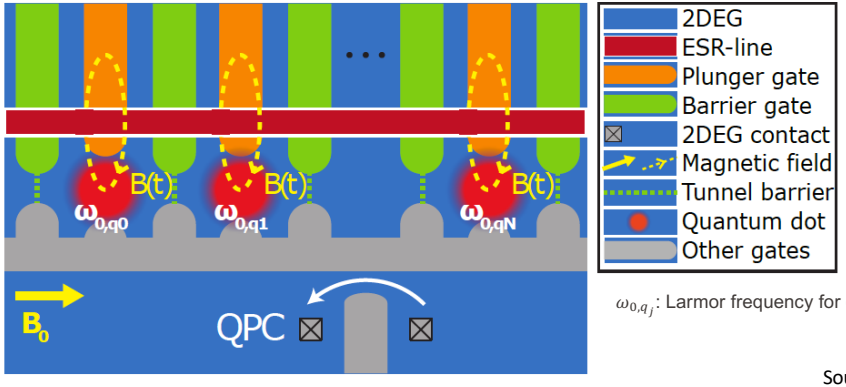

ω_{0,q_j}: Larmor frequency for qubit j

Source: Jeroen V. Dijk

Classical Control at RT (for ESR and EDSR)

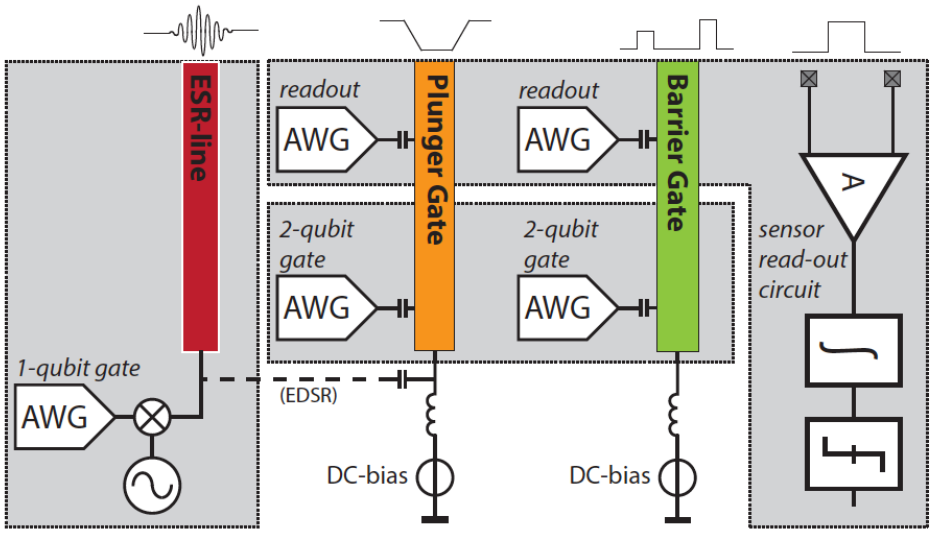

AWG: Arbitrary Waveform Generator
A: Amplifier

Source: Jeroen V. Dijk

Case Study for Single-Qubit Control

- The goal is a 99.9% fidelity for π rotation
- Given:
  - Typical Rabi frequency of 1MHz ($T_2^* = 120\mu s$)
  - FDMA scheme
  - $T_{nop} = T$
  - Larmor frequency $f_0 = 10$GHz
  - Frequency spacing: 1GHz
- Assuming:
  - Isotopically purified Si (<800ppm of ^{29}Si)
  - Amplitude: 2mV (1.4mV$_{RMS}$)

Source: Jeroen V. Dijk

Case Study for Single-Qubit Control (2)

- Following these specifications
  - Microwave envelope (amplitude and duration) can be generated with a sample rate of at least 150MS/s or a sample time of 6.7ns
  - Thus, the maximum inaccuracy is 3.3ns
  - The AWG can have a resolution of 8 bits, the full-scale swing is 4mV
  - Quantization step = 4mV/256 = 16μV
  - An effective number of bits (ENOB) of 6.5 bits is sufficient to meet the noise requirements
- The LO used for up-conversion needs a frequency resolution of ~20kHz, assuming -20dB/dec slope of phase noise.
- The SSB phase noise at 1MHz offset from the carrier needs to be less than -106dBc/Hz
- The phase inaccuracy needs to be < 0.64^{o}.

Source: Jeroen V. Dijk

Case Study Results (Single-Qubit Control)

	Value	Infidelity contribution to an operation	Infidelity contribution to idling
Frequency			
nominal	10 GHz	0.64×10^{-9} [a]	
spacing	1 GHz		1×10^{-6} [b]
inaccuracy	11 kHz	125×10^{-6}	308×10^{-6}
oscillator noise	11 kHz_{rms}	125×10^{-6}	308×10^{-6}
nuclear spin noise	1.9 kHz_{rms} [c]	3.6×10^{-6}	8.9×10^{-6}
wideband noise	12 μV_{rms}	125×10^{-6}	
Phase			
inaccuracy	0.64°	125×10^{-6}	31×10^{-6} [d]
Amplitude			
nominal	2 mV		
inaccuracy	14 µV	125×10^{-6}	
noise	14 μV_{rms}	125×10^{-6}	
off-spur	19 µV [e]		217×10^{-6}
off-noise	10 μV_{rms}		125×10^{-6}
Duration			
nominal	500 ns		
inaccuracy	3.6 ns	125×10^{-6}	
noise	3.6 ns_{rms}	125×10^{-6}	
		$F_{X,Y} = 99.9\,\%$	$F_I = 99.9\,\%$

Noise source	ENBW	Noise level
Frequency noise	2.5 MHz	$\mathcal{L}(1\,\text{MHz}) = -106\,\text{dBc/Hz}$
Wideband additive noise	2.9 MHz	$7.1\,\text{nV}/\sqrt{\text{Hz}}$
Amplitude noise	1.0 MHz	$14\,\text{nV}/\sqrt{\text{Hz}}$, SNR = −40 dB
Amplitude off-noise	2.0 MHz	$7.1\,\text{nV}/\sqrt{\text{Hz}}$

[a] Due to the RWA.
[b] Due to leakage in FDMA-setup using rectangular envelopes.
[c] From [61], $T_2^* = 120\,\mu s$.
[d] FDMA Z-corrections limit the idling operation.
[e] Equivalent to −41 dBc.

Source: Jeroen V. Dijk

Case Study Results (2-Qubit Control)

	Value	Infidelity contribution to an operation	Infidelity contribution to idling
Frequency			
spacing	1 GHz		
inaccuracy	11 kHz	77×10^{-6}	308×10^{-6}
oscillator noise	$11\,\text{kHz}_{\text{rms}}$	77×10^{-6}	308×10^{-6}
nuclear spin noise	$1.9\,\text{kHz}_{\text{rms}}$	2.2×10^{-6}	8.9×10^{-6}
Duration			
nominal	250 ns		
error	5.3 ns	281×10^{-6}	
Detuning energy			
nominal	0 mV (0 μeV, 0 GHz)		
error	12 mV (0.60 meV, 0.15 THz) $\sigma = 9.2\,\text{mV}_{\text{rms}}$ PSD = $2.9\,\mu\text{V}/\sqrt{\text{Hz}}$	281×10^{-6}	
Tunnel coupling			
nominal	0.71 GHz (2.9 μeV)		
error	7.5 MHz (31 neV)	281×10^{-6}	
off-value	78 MHz (0.32 μeV)		374×10^{-6}
		$F_{\text{cz}} = 99.9\,\%$	$F_{\text{I}} = 99.9\,\%$

	Value	Infidelity contribution to an operation	Infidelity contribution to idling
Frequency			
spacing	1 GHz		
inaccuracy	$11\,\text{kHz}_{\text{rms}}$	0.8×10^{-6}	308×10^{-6}
oscillator noise	$11\,\text{kHz}_{\text{rms}}$	0.8×10^{-6}	308×10^{-6}
nuclear spin noise	$1.9\,\text{kHz}_{\text{rms}}$	0.02×10^{-6}	8.9×10^{-6}
Duration			
nominal	25 ns		
error	0.58 ns	333×10^{-6}	
Detuning energy			
nominal	78 mV (3.9 meV, 0.95 THz)		
error	0.10 mV (5.1 μeV, 1.2 GHz) $\sigma = 0.10\,\text{mV}_{\text{rms}}$ PSD = $10\,\text{nV}/\sqrt{\text{Hz}}$	333×10^{-6}	
Tunnel coupling			
nominal	0.71 GHz (2.9 μeV)		
error	8.2 MHz (34 neV)	333×10^{-6}	
off-value	78 MHz (0.32 μeV)		374×10^{-6}
		$F_{\text{cz}} = 99.9\,\%$	$F_{\text{I}} = 99.9\,\%$

Table 3.4: Example specifications for the control electronics when operating a C-phase gate at no detuning (top) and at finite detuning (bottom). The PSD values provided assume a white spectrum with an ENBW of approximately 10 MHz ($\omega_{\text{op}} = 2$ MHz) when operating at no detuning and an ENBW of approximately 100 MHz ($\omega_{\text{op}} = 20$ MHz) at finite detuning. A nominal charging energy of 83 mV (4.1 meV, 1.0 THz) is assumed.

Source: Jeroen V. Dijk

Case Study for Single-Qubit Readout

- The goal is a 99.9% fidelity for π rotation
- Given:
  - Singlet-triplet energy splitting E_{ST} = 50meV
  - Optimum detuning: 83.2mV
- Assuming:
  - Isotopically purified Si (<800ppm of ^{29}Si)
  - Amplitude: 2mV (1.4mV$_{RMS}$)

Source: Jeroen V. Dijk

Case Study for Single-Qubit Readout (2)

- Following these specifications
  - 9-bit resolution to meet the accuracy of detuning
  - I_S = 400pA
  - $i_{n,S}$ = 57fA/$\sqrt{Hz}$
- Integration time of at least T_{read} = 0.6ns to achieve a SNR of 46dB for a probability of detection P_{detect} of 99.967% and a fidelity F of 99.9%.

Source: Jeroen V. Dijk

Case Study Results (Single-Qubit Readout)

	Value	Infidelity contribution to the read-out
Detuning energy		
nominal	83.2 mV (4.2 meV, 1.0 THz)	
error	0.24 mV (12 μeV, 2.8 GHz) $\sigma = 0.24\,\mathrm{mV_{rms}}$ PSD = 0.24 μV/√Hz	167×10^{-6}
Tunnel coupling		
nominal	39 MHz (0.16 μeV)	167×10^{-6}
		$P_{\mathrm{charge}} = 99.967\,\%$

	Value	Infidelity contribution to the read-out
Charge sensor		333×10^{-6}
		$P_{\mathrm{sense}} = 99.967\,\%$

	Value	Infidelity contribution to the read-out
Quantum Point Contact		
signal	400 pA	
noise	$53\,\mathrm{pA_{rms}}$, PSD = 57 fA/√Hz	222×10^{-6}
Readout Circuit		
input-referred noise	$26\,\mathrm{pA_{rms}}$, PSD = 28 fA/√Hz	111×10^{-6}
		$P_{\mathrm{detect}} = 99.967\,\%$

$P_{\mathrm{charge}} \cdot P_{\mathrm{sense}} \cdot P_{\mathrm{detect}}$	$F = 99.9\,\%$

Source: Jeroen V. Dijk

Derivations and Methods

- The qubit state satisfies Schrödinger's equation

$$i\hbar\frac{\partial|\psi\rangle}{\partial t} = H_{sys}\cdot|\psi\rangle,$$

where:

H_{sys} is the system Hamiltonian, which is a function of the electrical signals.

- For static control signals, the Hamiltonian is time-independent and the unitary operation describing the evolution after time T is trivially $U = e^{-iH_{sys}T}$ (assuming $\hbar$=1)

Derivations and Methods (2)

- For dynamic signals, such as for complex signal envelopes, we use the time-varying Hamiltonian $H(t)$, we have:

$$U \approx \prod_{n=N}^{0} e^{-i\,H(n\cdot\Delta t)\cdot\Delta t},$$

where:

Δt is the time step, which should be chosen to be small enough for the required accuracy of the approximation.

Derivations and Methods (3)

- To evaluate how close U is to the ideal U_{ideal}, the process fidelity is computed as:

$$F = \frac{1}{n^2} \cdot \left|\mathrm{Tr}\left(U_{ideal}^{\dagger} \cdot U\right)\right|^2,$$

where:

n is the dimension of the corresponding Hilbert space.

Trace: $\mathrm{Tr}(A) = \sum_{i=1}^{n} a_{ii} = a_{11} + a_{22} + \cdots + a_{nn}$.

$$A = \begin{pmatrix} a_{11} & a_{12} & a_{13} \\ a_{21} & a_{22} & a_{23} \\ a_{31} & a_{32} & a_{33} \end{pmatrix}.$$

Derivations and Methods (4)

- The qubit state rotates around the Z axis when an external magnetic field is applied.
- When using a RF signal tuned to a frequency equal to the Larmor frequency, the qubit appears stationary.
- Z rotations by θ_z can be obtained by halting the RF signal for time $T = \theta_z/\omega_0$.
- A phase error of $\Delta\varphi = \Delta\theta_z$, the fidelity of the rotation becomes:

$$F_{Z_\varphi} = 1 - \frac{1}{4} \cdot \Delta\varphi^2$$

Hamiltonian Describing Single Electron

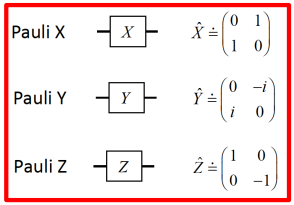

- Assuming again $\hbar = 1$, the Hamiltonian describing an electron under microwave excitation in the lab frame is:

$$H_{lab} = -\omega_0 \frac{\sigma_z}{2} + \gamma_e \cdot B(t) \frac{\sigma_x}{2},$$

where σ_x and σ_z are the Pauli matrices. ω_0 is the Larmor frequency.

- The AC magnetic field is:

$$\mathrm{B(t)} = 2/\gamma_e \cdot \omega_R(t)\cos(\omega_{mw} t + \varphi)$$

- In the rotating wave approximation (RWA), the Hamiltonian in the frame rotating with frequency ω_{mw} is:

$$H \approx (\omega_{mw} - \omega_0)\frac{\sigma_z}{2} + \omega_R\left[\cos(\varphi)\frac{\sigma_x}{2} - \sin(\varphi)\frac{\sigma_y}{2}\right]. \qquad (*)$$

- NB: The RWA is only valid when the Rabi frequency is much lower than the Larmor frequency ($\omega_R \ll \omega_0$).

Hamiltonian Describing Single Electron (2)

- From (*) we conclude that:
  - The fidelity is affected by frequency inaccuracy $\Delta\omega_{mw} = \omega_{mw} - \omega_0$ as:

$$F_{X,Y} = 1 - \frac{1}{2} \cdot \left(\frac{\Delta\omega_{mw}}{\omega_R}\right)^2 [1 - \cos(\theta)],$$

    where θ is the intended angle of rotation from $-\pi$ to π.

  - The fidelity is affected by the phase of the microwave signal, as:

$$F_{X,Y} = 1 - \frac{1}{2} \cdot (\Delta\varphi)^2 [1 - \cos(\theta)].$$

  - The fidelity is affected by the duration T of the microwave signal as:

$$F_{X,Y} = \cos^2\left(\frac{\theta}{2}\frac{\Delta T}{T_{ideal}}\right).$$

More Details in this Paper:

PHYSICAL REVIEW APPLIED **12,** 044054 (2019)

Impact of Classical Control Electronics on Qubit Fidelity

J.P.G. van Dijk,[1,2,*] E. Kawakami,[3] R.N. Schouten,[1,2] M. Veldhorst,[1,2] L.M.K. Vandersypen,[1,2,4] M. Babaie,[1] E. Charbon,[1,2,4,5] and F. Sebastiano[1]

[1] *QuTech, Delft University of Technology, P.O. Box 5046, 2600 GA Delft, Netherlands*
[2] *Kavli Institute of Nanoscience, P.O. Box 5046, 2600 GA Delft, Netherlands*
[3] *Okinawa Institute of Science and Technology, Okinawa 904-0412, Japan*
[4] *Intel Corporation, 2501 NW 229th Ave, Hillsboro Oregon 97124, USA*
[5] *École Polytechnique Fédérale de Lausanne, Case postale 526, CH-2002 Neuchâtel, Switzerland*

(Received 17 March 2018; revised manuscript received 30 May 2019; published 24 October 2019)

Quantum processors rely on classical electronic controllers to manipulate and read out the state of quantum bits (qubits). As the performance of the quantum processor improves, nonidealities in the classical controller can become the performance bottleneck for the whole quantum computer. To prevent such limitation, this paper presents a systematic study of the impact of the classical electrical signals on the qubit fidelity. All operations, i.e., single-qubit rotations, two-qubit gates, and readout, are considered, in the presence of errors in the control electronics, such as static, dynamic, systematic, and random errors. Although the presented study could be extended to any qubit technology, it currently focuses on single-electron spin qubits, because of several advantages, such as purely electrical control and long coherence times, and for their potential for large-scale integration. As a result of this study, detailed electrical specifications for the classical control electronics for a given qubit fidelity can be derived. We also discuss how qubit fidelity is affected by the limited performance of the general-purpose room-temperature equipment typically employed to control the few qubits available today. Ultimately, we show that tailor-made electronic controllers can achieve significantly lower power, cost, and size, as required to support the scaling up of quantum computers.

DOI: 10.1103/PhysRevApplied.12.044054

Thank you

T. Haensch